A Cell-Based Model Exhibiting Branching and Anastomosis during Tumor-Induced Angiogenesis

Amy L. Bauer,* Trachette L. Jackson,* and Yi Jiang†
*Department of Mathematics, University of Michigan, Ann Arbor, Michigan; and †Theoretical Division, Los Alamos National Laboratory, Los Alamos, New Mexico

ABSTRACT This work describes the first cell-based model of tumor-induced angiogenesis. At the extracellular level, the model describes diffusion, uptake, and decay of tumor-secreted pro-angiogenic factor. At the cellular level, the model uses the cellular Potts model based on system-energy reduction to describe endothelial cell migration, growth, division, cellular adhesion, and the evolving structure of the stroma. Numerical simulations show: 1), different tumor-secreted pro-angiogenic factor gradient profiles dramatically affect capillary sprout morphology; 2), average sprout extension speeds depend on the proximity of the proliferating region to the sprout tip, and the coordination of cellular functions; and 3), inhomogeneities in the extravascular tissue lead to sprout branching and anastomosis, phenomena that emerge without any prescribed rules. This model provides a quantitative framework to test hypotheses on the biochemical and biomechanical mechanisms that control tumor-induced angiogenesis.

INTRODUCTION

Tumor-induced angiogenesis is the formation of new blood vessels from existing vasculature in response to chemical signals from a tumor. Angiogenesis marks the pivotal transition from benign solid tumor growth to vascular growth, a more progressive and potentially fatal stage of cancer beyond which cancer becomes extremely difficult to treat, existing therapies become ineffective and survival rates decrease (1). Angiogenesis is a complex process, involving multiple time scales and intricate interplay between biochemical and biomechanical mechanisms, including cell-cell and cell-matrix interactions, cell surface receptor binding, and intracellular signaling pathways. The sequential morphogenetic processes required for angiogenesis to occur are well known and a review of these follows; however, what is still not completely understood is how cellular and molecular mechanisms are coordinated to control these processes. In this work, we present a cell-based modeling framework of tumor-induced angiogenesis designed to address these questions of mechanism. An understanding of the principal underpinnings driving angiogenic processes will advance efforts aimed at the development of new therapies for treating cancer and other angiogenesis-dependent diseases.

Tumor-induced angiogenesis

To ensure its sustained growth, a tumor must acquire a supply of nutrients and the ability to export metabolic waste. It does this by recruiting new blood vessels from the nearby existing vasculature. Circulating endothelial precursors, shed from the vessel wall or mobilized from bone marrow can also contribute to tumor angiogenesis (2). Tumor cells can also grow around an existing vessel to form a perivascular cuff (3). Oxygen-deprived, or hypoxic, tumor cells are responsible for releasing a wide variety of polypeptide angiogenic factors that stimulate vessel growth toward the tumor (4). These angiogenic factors diffuse through the surrounding tissue, setting up a chemical gradient between the tumor and any existing vasculature. Various molecular players are now known to be involved in these different mechanisms of vascular growth (5). Among these, members of the vascular endothelial growth factor (VEGF) and angiopoietin family have a prominent role (6). When VEGF reaches the blood vessel, it triggers a cascade of events. Fig. 1 illustrates the major VEGF-mediated events that occur during early angiogenesis. Endothelial cells, which form the interior lining of blood vessels, have cell surface receptors specific to VEGF (7). Endothelial cells are activated via two receptor tyrosine kinases, FMS-like tyrosine kinase-1 and fetal liver kinase-1, which are often referred to as VEGFR1 and VEGFR2, respectively (8). VEGF binds to these receptors triggering intracellular signaling pathways. One example is the VEGF-Bcl2-CXCL8 signaling pathway, which mediates pro-angiogenic and pro-survival phenotypes in endothelial cells (9). Intracellular signaling leads to gene transcription, the production of enzymes and angiogenic factors, increased cell survival, migration, and proliferation (10).

At the onset of angiogenesis, endothelial cell activation results in increased vascular permeability (11) and the production of proteases that locally degrade the basement membrane of the blood vessel (12,13). This breakdown of the basement membrane enables the endothelial cells to migrate into the extracellular matrix of the extravascular connective tissue, hereafter referred to as stroma. The extracellular matrix (ECM) is a major component of the stroma

Submitted November 21, 2006, and accepted for publication January 11, 2007.

Address reprint requests to Y. Jiang, Tel.: 505-665-5745; E-mail: jiang@lan1.gov.

0006-3495/07/05/3105/17 $2.00 doi: 10.1529/biophysj.106.101501

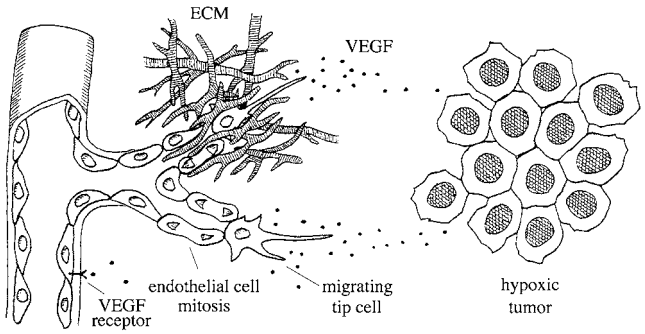

FIGURE 1 An illustration of early events in sprouting angiogenesis: VEGF-mediated endothelial cell activation and degradation of the basement membrane, subsequent migration and invasion into the stroma led by tip cells extending filopodia, cell division, and endothelial cell interaction with extracellular matrix fibers. This illustration emphasizes that the processes involved in angiogenesis are controlled at the level of individual cells. In this context, cellular dynamics are a discrete process and a cell-based model is a better description over continuous models, which deal with cell densities.

and plays a central role in cellular migration, cell shape, and orientation (14). The ECM is a meshlike molecular network composed of fibrous collagen proteins, elastin, adhesive proteins, such as fibronectin, and proteoglycans (see Fig. 1) (15). To reach the tumor, endothelial cells must navigate the stroma. Activated endothelial cells also upregulate additional cell surface receptors integrins, which regulate cellular adhesion to matrix molecules (16). To facilitate their migration, endothelial cells have the ability to condition the ECM by producing a number of different proteolytic enzymes that degrade specific ECM proteins (12,13). Two such proteases are plasminogen activators and matrix metalloproteinases. Plasminogen activators are crucial for the degradation of fibronectin and laminin, whereas matrix metalloproteinases degrade collagen and elastin (12,17).

There is substantial empirical evidence indicating that VEGF induces endothelial cell migration (18–21). One means of endothelial cell migration is by positive chemotaxis, which is directed motility up chemical gradients. Using a Boyden chamber assay, Cao et al. (21) showed that VEGF elicits a strong chemotactic response in human umbilical vein endothelial cells. In an in vitro study of two populations of porcine aortic cells, one cell line expressing only VEGFR1 and the other only VEGFR2 (22) demonstrated that VEGFR2 was solely responsible for VEGF-mediated chemotaxis. Endothelial cell migration also occurs along positive gradients of cellular adhesion sites that are naturally present in the ECM (23), or haptotaxis. Endothelial cell degradation of collagen and fibronectin can create new or amplify existing local adhesive gradients, which also mediates endothelial cell haptotaxis (24).

VEGF can regulate very different cellular responses resulting in phenotypically distinct populations of endothelial cells. In murine retinal angiogenesis, it was shown that the sprout tip consisted of a single endothelial cell that responded to VEGF solely by gradient-directed migration (no proliferation) and that VEGF-induced proliferation occurred only in the cells comprising the sprout stalk, or stalk cells (19). The mitogenicity of VEGF on endothelial cells has also been well substantiated (7,18,21,25). From the experiments of Waltenberger et al. (22) described above, it was again shown that VEGFR2 was the only receptor implicated in VEGF-stimulated endothelial cell mitosis. During angiogenesis, endothelial cell proliferation provides the additional cells necessary for the sprout to grow and extend further into the stroma toward the tumor (see Fig. 1) (17,26,27). As the new sprout approaches the tumor, branches develop when the sprout tip splits in two and closed loops can be formed when neighboring sprouts fuse together, a process called anastomosis.

Newly formed angiogenic sprouts are initially immature (8). Immature sprouts lack a basement membrane and are not yet capable of supporting blood flow (17). For sprouts to mature, many other processes must first occur, including lumen and vacuole formation, the recruitment of specialized cells, and the reconstruction of a basement membrane. Endothelial cells must abandon their invasive phenotype and reassociate with the ECM via cell surface integrins (28). In vitro experiments of human endothelial cells in three-dimensional collagen matrices showed that vacuole and lumen formation depend on collagen-binding integrin $\alpha 2\beta 1$ (29). These studies showed that intracellular vacuoles enlarge and coalesce to create a luminal compartment. Endothelial cells further associate and develop lumens at sites of cell-cell contact, thereby generating tubular structures. Pericytes and smooth muscle cells are recruited by endothelial cells. These cells contribute to vessel stability and maturation by inhibiting endothelial cell proliferation and promoting new basement membrane synthesis (30). The result is a fully mature vessel capable of blood transport and thus nutrient delivery to the tumor.

Although the fundamental processes that occur during angiogenesis are well established, there is still considerable ambiguity and debate regarding how biochemical and biomechanical mechanisms are coordinated to control vascular development. Recent efforts in experimental research have intensely focused on advancing our understanding of these mechanisms in hopes of discovering novel anti-angiogenesis therapies. However, as new experimental assays capable of examining the cellular and molecular level dynamics during angiogenesis are developed, discordant data have been published. Below we review some of the experimental observations that have generated confusion and given rise to dogma. Specific hypotheses are then formulated and tested with our computational model.

VEGF isoforms

A common perception has been that a freely soluble form of VEGF is solely responsible for both the activation and the differentiation of function seen in endothelial cells during tumor-induced angiogenesis. However, this belief is being

revised as experiments demonstrate that sequential activation of various endothelial cell surface receptors by multiple ligands are required for angiogenesis. Experiments show that the same VEGF receptor (VEGFR2) is responsible for mediating very different cellular functions, including endothelial cell growth, mitogenesis, migration, and increased survival (22,31). Some studies propose that the outcome of VEGFR2 signaling depends on the particular VEGF isoform present (19,31). The effects of different VEGF isoforms on vascular structure have been examined and significantly different capillary morphologies were observed in the presence of matrix bound versus soluble VEGF (32). To further complicate matters, other investigations have demonstrated that local growth differentials can exist even in areas saturated with soluble angiogenic factor (14). We intend to address the role various VEGF isoforms play in the guidance and formation of capillary sprouts, such as: How does the binding and release of bioavailable VEGF affect local chemical gradients? What are the respective effects on vascular structure of diffusible and matrix-bound VEGF? What mechanisms induce proliferation in one cell but not its neighbor? And can the presence of matrix bound or cleaved soluble angiogenic factors distinguish a proliferating region, possibly explaining both the observed growth differentials and the reports of different proliferating regions?

Proliferating region

There is convincing experimental evidence that endothelial cell proliferation is a necessary process for tumor vascularization (27). It is generally believed that during angiogenesis, proliferation occurs right behind the tip cell and only after the endothelial cells have already migrated into the stroma some distance (17,27). Presently, however, discrepancies persist concerning the precise location of the proliferating cells during angiogenesis. Experimental models have reported mitotic activity occurring at the base of a newly formed sprout (17,33), some distance behind the sprout tip (17,34), localized immediately behind the sprout tip cell (17,27) and at the tip (35,36). Another area where contradictory experimental data exist is whether proliferation and migration are mutually exclusive events. Some studies have reported that proliferation and migration are segregated cellular functions (19,35), whereas more recent evidence suggests that a proliferating cell does indeed migrate (33). Cell-based modeling can assist in our understanding and synthesis of such empirical data because it allows us to study the impact of the location of the proliferating region on capillary formation. To the best of our knowledge, no other model has explored the effects of various proliferating regions or segregation of function on capillary morphology.

Composition of stroma

The location of the tumor dictates the environment in which endothelial cells must survive and migrate. Depending on the tissue, the density of the matrix and the variety of other cells that make up the stroma can vary a great deal. It is widely accepted that cellular interactions with the ECM and the location of the tumor have a significant impact on new capillary sprout formation and morphology. Therefore understanding how the ECM modulates angiogenic processes has commanded considerable attention in experimental research. However, there is still speculation concerning the precise mechanisms involved; for example, what role does the ECM play in endothelial cell function? How are growth differentials between neighboring endothelial cells established? How is sprout branching initiated? And can the composition of the stroma be manipulated to inhibit angiogenesis? A more in-depth investigation of the role of the composition and structure of the stroma on capillary formation is needed and cell-based modeling provides a forum for such studies.

Our presentation of and discussion on conflicting experimental data suggest the following research hypotheses:

H1. The presence of matrix-bound and soluble VEGF results in different vascular morphologies.

H2. The location of the proliferating region of cells has an impact on capillary morphology and the rate of capillary sprout extension.

H3. The composition of the stroma, such as ECM density and the presence of other tissue cells, influences endothelial cell migration and capillary formation during angiogenesis.

MATHEMATICAL MODELS OF ANGIOGENESIS

A great number of factors must be tightly coordinated to promote tumor-induced angiogenesis. No single model has yet incorporated every aspect of every process involved in sprouting angiogenesis, nor is this level of complexity necessary for a model to be useful or predictive. Focused investigations on particular mechanisms or processes have led to the development of models of angiogenesis. Growth factor-mediated protease production was modeled, incorporating an important biochemical mechanism for ECM degradation and regulation of endothelial cell proliferation (37,38). Cell-receptor-level treatment of this critical biochemical pathway derived from first-principle Michaelis-Menten chemical kinetics was a significant contribution to modeling angiogenesis. Other advances in modeling are being achieved at a more macroscopic level through the development of a dynamic adaptive tumor-induced angiogenesis model (39), which took into account hemodynamic forces such as shear stress and variable blood viscosity in the dynamic remodeling of vascular architecture. These and other existing mathematical models offer many insights into the processes driving angiogenesis and highlight necessary conditions for angiogenesis to occur, such as endothelial cell proliferation, haptotaxis, and chemotaxis (40,41), by concentrating on very specific mechanisms influencing capillary sprout development.

Discrete and continuum models of angiogenesis that model sprout tip cells or cell densities are predicated on the fact that the tip cell governs the motion of the entire capillary sprout. Consequently, these models assume that the rest of the cells in the capillary sprout are inactive. However, the endothelial cells in the sprout dynamically contribute to vascular structure through the forces of cellular adhesion, cell signaling, and the local restructuring of the ECM (42). To reproduce realistic vascular networks, these models must assign probabilities to rules for branching (39–41,43). Thus, branching was not an inherently emergent phenomenon, but a prescribed one. Vascular networks have also been successfully generated by modeling the mechanical properties of the ECM, such as elasticity and stiffness. A model incorporating both chemical and mechanical forces, notably the traction that endothelial cells exert on a viscoelastic ECM, was able to produce vascular patterns that resemble those observed in the in vitro experiments (44). However, this work only considered tractile forces in a continuum model framework and did not fully investigate the role of chemotaxis and sprouting vessels in tumor-induced angiogenesis. Another leading effort in modeling tumor-induced angiogenesis is described in Sun et al. (45), where they explicitly modeled the anisotropy and heterogeneity of the ECM and were able to capture the dendritic structure of capillary network formation. However, sprout branching still only occurred as a result of imposed rules. A new branch was generated when both the age of the sprout is above some prescribed age and the variation of the tip velocity transverse to the existing sprout orientation is greater than a certain threshold value. Although the structure of the ECM was incorporated into their model, direct endothelial cell-matrix interactions were not, and consequently, the model was unable to capture the individual cell dynamics that allow cells to respond differently according to their specific local microenvironment.

Cell-based modeling

Fig. 1 emphasizes that the processes involved in angiogenesis happen at the level of individual cells. A cell-based model is able to account for individual cell interactions with and influence on their local environment. Consequently, cell-specific biochemical and biomechanical dynamics are easily incorporated. In addition, because the typical sprout is only a few endothelial cells wide, cell-based modeling provides a better description of the cellular dynamics during early angiogenesis than continuum models, which deal with cell densities. In this first report of our new model, we do not attempt to introduce every dynamic known to influence angiogenesis. The primary aim of our investigation is to understand the roles of cell-cell and cell-matrix interactions on sprouting angiogenesis. We therefore focus only on those specific cell-cell and cell-matrix dynamics that occur at the onset of angiogenesis. We also incorporate several key biochemical dynamics: 1), VEGF binding to, internalization, and recycling of endothelial cell surface receptors; 2), VEGF-mediated cellular activation, migration, and proliferation; and 3), proteolytic extracellular matrix degradation. Another advantage to cell-based modeling is that adding another scale to the system, for example by incorporating intracellular signaling as was done in Jiang et al. (46), is a relatively straightforward extension of the model. Intracellular events downstream of VEGF binding to endothelial cell surface receptors are not crucial to our present investigations of cell-cell and cell-matrix interactions and therefore are not explicitly treated in this model. However, intracellular signaling will be an important consideration for more in-depth investigations of the biochemical mechanisms controlling angiogenesis, and the results obtained here will be used to help discern which intracellular signaling pathways are necessary to include in future extensions of this model. In addition, because our attention is on the early events in sprouting angiogenesis, our simulated sprouts are not fully mature vessels that are capable of supporting blood flow. However, as was shown in Kearney et al. (33), blood flow is not required for branching and anastomosis to occur and thus, at this stage, we do not consider the effects of blood flow in our model.

In this work, we concentrate on: 1), developing a cell-based approach to modeling growth, division, and migration during early angiogenesis; 2), incorporating the key biochemical and biomechanical interactions occurring between endothelial cells and the ECM; and 3), investigating the mechanisms responsible for generating realistic capillary structures, including branching and anastomosis, without a priori prescribing rules and probabilities to these events. Our model is distinct from previous models of tumor-induced angiogenesis in several ways. First, this model captures single cell biochemical and biomechanical dynamics allowing individual cells to interact with and influence their local environment. This model constitutes the first cell-based model of tumor-induced angiogenesis. Second, we explicitly model the stroma, including structural variations, such as the anisotropy of the matrix fiber distribution and tissue specific cells. Third, we distinguish between sprout tip and stalk cells and incorporate the distinct behavior each cell phenotype exhibits. Finally, our major result is that this model is capable of simulating capillary sprout branching and anastomosis, larger-scale structures that emerge only as a result of the featured cellular and molecular level dynamics; no rules specifically incorporating branching or anastomosis are imposed.

This article is organized in the following manner. We first present our new cell-based model of tumor-induced angiogenesis. We then present results from numerical simulations demonstrating the capability of this model to produce realistic capillary structures. We further use the model to test the hypotheses formulated above and report our findings. A discussion and summary conclude our communication.

CELL-BASED MODEL OF TUMOR-INDUCED ANGIOGENESIS

Model architecture

The processes involved in angiogenesis naturally suggest a three-tier time and length scale architecture. We have developed a cell-based model structured in terms of these multiple scales by incorporating extracellular and intercellular environments. An intracellular level can be added to incorporate signaling pathways that control cell cycle and other signaling dependent decisions that occur inside the cells. This is the subject of future work. Our model utilizes the advantages of both discrete and continuous modeling. At the extracellular level, a partial differential equation describes diffusion, uptake, and half-life decay of tumor-secreted VEGF. At the cellular level, a discrete lattice Monte Carlo model (the cellular Potts model) considers cell migration, growth, proliferation, cellular adhesion, and extracellular matrix degradation. The extra- and intercellular environments are integrated and directly impact each other.

Model domain and geometry

We initiate the simulations with a single endothelial cell, which has degraded the basement membrane of the primary blood vessel that lies adjacent to the left hand boundary. Adjacent to the right-hand boundary, an avascular tumor is situated which delivers VEGF to the stroma. Fig. 2 shows the initial configuration and geometry of the domain. Using a two-dimensional domain provides a first approximation to capillary sprout formation in vivo and allows us to compare our results with both planar experimental models (e.g., (32,36,47) and other two-dimensional computational models (41,43,45). Our model has the flexibility to examine capillary sprout development at different length scales. The avascular cornea of the rodent eye is a classical angiogenesis assay, which allows the process of neovascularization to occur over long distances (1–2 mm) (35,48). However, tumors forming in other tissues, for example in the lung, brain, stomach, and breast, are typically much closer to the existing vasculature. Since our interest is on individual cell interactions during early sprouting angiogenesis, and sprout initiation and branching have been shown to occur over distances ranging from 20 to 100 μm (32,33), in our model, the distance between the parent blood vessel and the tumor is $\sim$165 μm. This distance is slightly larger than the diffusion limit for oxygen ($\sim$100 μm). We choose this length scale so that we can focus on cell-cell and cell-matrix interactions, to replicate the hypoxic conditions that may arise in vivo, and to allow sufficient space for the new sprouts to grow 100 μm without encountering an artificial boundary.

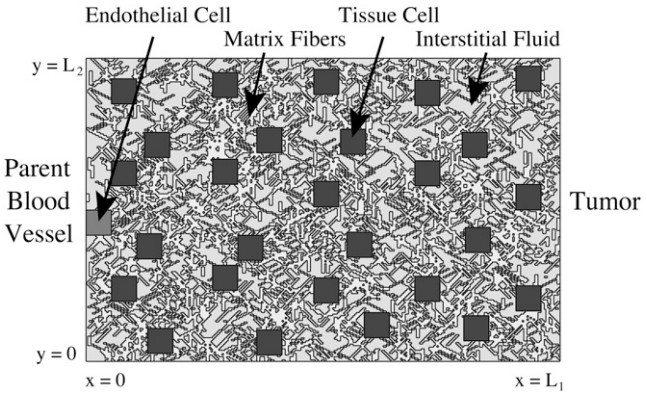

FIGURE 2 The geometry of the initial domain. An EC bud (*dark gray*) protrudes into the domain from the parent blood vessel on the left; an avascular tumor resides outside the domain on the right-hand side and supplies VEGF to the stroma. The space between represents the stroma and is composed of extracellular matrix fibers (*light gray*), tissue-specific cells (*black*), and interstitial fluid (*gray*).

Extracellular environment

The evolution of VEGF sets up a chemical gradient between the tumor and the parent blood vessel and constitutes the extracellular environment to which the endothelial cells respond. VEGF is secreted by the tumor and diffuses through the stroma where it decays at a constant rate and is taken up by endothelial cells. Mathematically, the spatial profile of VEGF satisfies a partial differential equation of the form

$$\frac{\partial V}{\partial t} = D\nabla^2 V - \lambda V - B(x, y, V), \tag{1}$$

where $V = V(x, y, t)$ denotes VEGF concentration. The coefficient of diffusivity for VEGF in tissue, $D > 0$, is assumed to be homogeneous throughout the simulation domain. The rate VEGF decays, $\lambda > 0$, is also assumed to be constant, and $B(x, y, V)$ is a function describing endothelial cell binding and uptake of VEGF.

The maximum amount of VEGF that can be bound and internalized by an endothelial cell per unit of time is denoted by β. To compute β, we consider the number of VEGF receptors per endothelial cell and the rate at which VEGF-receptor complexes can be internalized and surface receptors recycled. Vascular endothelial cells express both VEGFR1 and VEGFR2. While VEGFR2 is VEGF-specific, VEGFR1 is not and can bind adhesion molecules and other growth factors (49). However, in this model, we do not consider multiple VEGF isoforms or growth factors, or the explicit binding of adhesion molecules, both of which compete for available binding sites. Thus, in our calculation of β, we use the total number of VEGFR1 and VEGFR2 receptors per cell (311,200 (50)), an instantaneous VEGF-receptor complex internalization rate of 4.3×10^{-4} per second, and 45 kDa as the molecular weight for $VEGF_{165}$ (7,49). The value of β is given in Table 1. Receptor binding occurs very rapidly compared to the timescale of endothelial cell migration and proliferation. Thus, we assume that an endothelial cell instantly binds an amount of VEGF equal to the lesser of available

TABLE 1 Table of parameters

Parameter	Symbol	Dimensions	Model value
VEGF diffusion	D	L^2/T	3.6×10^{-4} cm^2/h (62)
VEGF decay	λ	T^{-1}	0.6498 h^{-1} (62)
VEGF uptake	β	M/cell/T	0.06 pg/EC/h (49,50,63)
VEGF source	S	M/L	0.035 pg/pixel (4,46)
Activation threshold	v_a	M	0.0001 pg
Proliferation threshold	v_p	M	0.005 pg
Adhesion			
EC–EC	J_{ee}	E/L	1
EC–fluid	J_{ef}	E/L	32
EC–matrix	J_{em}	E/L	16
EC–tissue	J_{et}	E/L	31
Fluid–fluid	J_{ff}	E/L	35
Fluid–matrix	J_{fm}	E/L	35
Fluid–tissue	J_{ft}	E/L	32
Matrix–matrix	J_{mm}	E/L	5
Matrix–tissue	J_{mt}	E/L	30
Tissue–tissue	J_{tt}	E/L	2
Membrane elasticity			
EC*	γ_e	E/L^4	1.0
Matrix	γ_m	E/L^4	0.4
Fluid	γ_f	E/L^4	0.1
Tissue cell*	γ_t	E/L^4	1.2
Chemotaxis*	μ	E/conc	-1.5×10^5
Boltzmann temperature	kT	E	0.01

Dimensions are given in terms of L = length, T = time, M = mass, and E = energy. For instance, the adhesion terms have dimensions of energy per unit length of cell membrane. An asterisk (*) designates a parameter that has been varied across numerical experiments; all other parameters were held fixed. The exact parameter values used in a simulation are given in the discussion corresponding to that experiment. Unless otherwise noted, all simulations used the same parameter set, initial configuration of matrix fibers and tissue cell distribution, and follow the assumptions described in the previous section. *EC* denotes endothelial cell.

chemical concentration V or the maximum amount that can be bound to endothelial cell surface receptors and internalized, β. This function is given by

$$B(x,y,V)=\begin{cases}\beta, & \text{if } \beta \le V \text{ and } \{(x,y)\subset \text{endothelial cell}\};\\ V, & \text{if } 0 \le V < \beta \text{ and } \{(x,y)\subset \text{endothelial cell}\};\\ 0, & \text{if } \{(x,y)\not\subset \text{endothelial cell}\}.\end{cases}$$

Initially, there is no VEGF in the stroma. The amount of VEGF supplied to the right-hand boundary of the domain was estimated by assuming that in response to a hypoxic environment, quiescent tumor cells secrete a constant amount of VEGF and that VEGF decays at a constant rate. It is reasonable to assume that the concentration of VEGF within the tumor has reached a steady state and therefore that a constant amount of VEGF, denoted S, is available at the boundary of the tumor. VEGF secretion rates for hypoxic human cancer cells were taken from experiments (4) and the number of quiescent cells secreting VEGF was estimated based on the total number of quiescent cells in an avascular tumor as measured in Jiang et al. (46). At a distance of 165 μm and given that an avascular tumor grows to ~1–2 mm in diameter (28), the supply of VEGF from the tumor can be approximated by a line source. Accordingly, the following initial and boundary conditions were used:

$$V(x,y,0)=0,$$
$$V(0,y,t)=0,\quad V(L_1,y,t)=S,\quad V(x,0,t)=V(x,L_2,t).$$

These initial and boundary conditions for VEGF have frequently been employed in previous models of tumor-induced angiogenesis (43,51,52). A dimensional analysis indicates that the concentration of VEGF in the stroma will also very quickly reach a steady-state profile due to the fast diffusion. Numerical computations confirm this. Consequently, the steady-state solution is a good approximation to Eq. 1 and we use the steady-state VEGF profile as an initial condition for the discrete model as was similarly done in the literature (41,43).

Modeling the stroma and extracellular matrix

The explicit modeling of the stroma and the extracellular matrix fibers is a novel feature of this model. The stroma is composed of matrix fibers, interstitial fluid, and tissue-specific cells creating an inhomogenous composition and structure. We include tissue cells in our model to mimic a more anatomically accurate extracellular environment for the growing and migrating endothelial cells. The properties associated with these cells are tissue-specific and depend on the particular biological processes being studied. For example, specialized cells, such as mast cells, fibroblasts, macrophages, or pericytes, could be modeled to capture the effects of other guidance cues on sprout formation or to examine their roles in sprout maturation and stability. Our current focus is to study how the composition of the stroma affects sprout morphology and migration, and therefore, at this stage a ''general'' tissue cell is modeled to provide an additional level of structure to the stroma. We assume that tissue cells are roughly the same size as an endothelial cell (15), are immobile, and are more difficult to invade than matrix fibers and interstitial fluid. Consequently, tissue cells compete for space and create intercellular pressure on and resistance to the migrating and proliferating endothelial cells. Matrix fibers comprise ~37% of the stroma and the architecture of the ECM is anisotropic, with regions of varying densities (15). A single collagen fibril is ~300-nm long and 1.5-nm wide and is substantially smaller than an endothelial cell, which is ~10 μm in diameter (15). Thus, to model the meshlike anisotropic structure of the ECM, we assume that many individual collagen fibrils and other matrix proteins are bound together constituting larger cords or bundles of matrix fibers that have been estimated to be between 100 and 1000-nm thick (53). We randomly distributed 1.1-μm-thick fiber bundles at randomly chosen discrete orientations ranging from 0 to 180° until 37% of the stroma was occupied.

Cellular Potts model for cellular dynamics

The processes involved in new capillary formation occur at the level of individual cells. Accordingly, we use the cellular Potts model to model the interactions between endothelial cells or between an endothelial cell and the stroma (matrix fibers, tissue cells, and interstitial fluid). The cellular Potts model is a discrete lattice Monte Carlo model developed by Glazier and Graner and is based on an energy minimization principle (54). The cellular Potts model has already been used to model a multitude of biological phenomena including differential adhesion-driven cell rearrangement (54), cellular differentiation and growth of tissues (55), fruiting body formation of *Dictyostelium* (56), avascular tumor growth (46), cancer invasion (57), and vasculogenesis (58, 59).

In this work, we extend the cellular Potts model to simulate tumor-induced angiogenesis. Our work is distinct from that presented in the literature (58,59), which modeled the reorganization of randomly dispersed cells into a vascular network pattern, simulating in vitro vasculogenesis. In contrast, our work focuses on the processes that generate the sprouting of new capillaries from a preexisting vasculature in vivo (angiogenesis). Moreover, our model considers cell growth and division, dynamics that are not modeled in the literature (58,59), and we explicitly model the ECM, a component critical to vascular formation.

The cellular Potts model partitions the computational domain into endothelial cells, matrix fibers, tissue cells, and interstitial fluid which are situated on a lattice and are denoted by type $\tau = \{e, m, t, f\}$, respectively. To account for individual cells, each cell is further associated with a unique identifying number, denoted by σ, that is assigned to every lattice site occupied by that entity (see Fig. 2 in (56) for an example). Matrix fibers and interstitial fluid are collectively identified by 1 and 0, respectively. Under this framework, each entity has a finite volume, a deformable shape, and competes for space. Intercellular interactions occur only at the cell's surface and have a cell-type-dependent surface (or adhesion) energy given by $J_{\tau,\,\tau'}$, which is a measure of the coupling strength between the entities τ and τ'. Cellular dynamics are characterized by an equation for total energy given by

$$E = \sum_{\text{sites}} J_{\tau,\tau'}(1-\delta_{\sigma,\sigma'}) + \sum_{\text{cells}} \gamma_\tau \left(a_\sigma - A_\sigma^{\mathrm{T}}\right)^2. \qquad (2)$$

The first term in Eq. 2 is the contribution to total energy resulting from cell adhesion at cell surfaces. The second term takes into account the fact that cell growth and deformation require energy, where a_σ denotes cell σ's current volume and A_σ^{T} is a designated ''target'' volume. We assume that the target volume of an endothelial cell undergoing mitosis is the volume that it would grow to in the absence of external forces and given sufficient nutrition, and is designated as twice its initial volume.

Additionally, we know that VEGF acts as a chemoattractant for endothelial cells (20). The effective energy required for chemotaxis, $\Delta E_{\text{Chemotaxis}}$, can be derived as follows: In our model, cell movement is governed by energy gradients and, over time, cells move to reduce the total energy of the system. Empirical evidence indicates that VEGF concentration gradients induce endothelial cells to move in the direction of increasing concentration with a velocity proportional to the VEGF gradient. Because the cells must move through the highly viscous ECM, their motion is overdamped and the force required for motion is proportional to velocity, $\vec{F}_{\text{Chemotaxis}} \propto \vec{v}$. Consequently, the force is proportional to the chemical gradient. We can construct an effective chemotaxis potential that is proportional to the local chemical gradient:

$$\Delta E_{\text{Chemotaxis}} = \mu_\sigma [V(\vec{x}) - V(\vec{x}')]. \qquad (3)$$

The parameter $\mu_\sigma < 0$ is the effective chemical potential, which influences the strength of chemotaxis relative to other parameters in the model. The values $\vec{x}'$ and $\vec{x}$ represent the two neighboring lattice sites randomly selected during one trial update in a Monte Carlo step, which is described in detail below.

The cellular Potts model evolves in time using repeated probabilistic updates of unique cell identification numbers, σ, on the lattice. Procedurally, a lattice site, $\vec{x}$, is selected at random and assigned the σ from one of its unlike second nearest neighbors, $\vec{x}'$, which has also been randomly selected. The total energy of the system is computed before and after the proposed update. If the total energy of the system is reduced as a result of the update, the change is accepted. If the update increases the energy of the system, we accept the change with a Boltzmann probability. Thus the probability of accepting an update is given by

$$P_{\text{acceptance}} = \begin{cases} 1, & \text{if } \Delta E < 0; \\ e^{-\Delta E/kT}, & \text{if } \Delta E \geq 0, \end{cases}$$

where ΔE is the change in total energy of the system as a result of the update, k is the Boltzmann constant, and T is the effective temperature that corresponds to the amplitude of cell membrane fluctuations. This probability influences the likelihood of energetically unfavorable events taking place (57). A total of n proposed updates, where n is the number of sites on the lattice, constitutes one Monte Carlo step and is the unit of time used in the model.

In the model, endothelial cells will move to promote stronger over weaker adhesive bonds, shorter over longer cell boundaries, and toward regions of higher chemical concentrations. Only endothelial cells are allowed to grow, move and invade; ECM, tissue-specific cells and interstitial fluid do not grow or actively invade each other or endothelial cells. Endothelial cells interact both mechanically and biochemically with the ECM. Effective mechanical forces exerted on the ECM by endothelial cells as they migrate are incorporated as a result of the matrix fibers' resistance to compression given by γ_{m}. Biochemical interactions include VEGF binding to, uptake by, and activation of endothelial cells, endothelial cell

matrix degradation, and the chemical bonds between endothelial cells and between endothelial cells and matrix fibers, which are accounted for by J_{ee} and J_{em}, respectively. Haptotaxis is naturally incorporated through this adhesion term whenever an endothelial cell interacts with a matrix fiber. The endothelial cells also interact with the tissue cells via surface adhesion and competition for space. Each endothelial cell additionally carries its own internal cell clock, which is used to determine where the cell is in its mitotic cycle and whether or not cell division can occur. The endothelial cell cycle is not explicitly modeled, but this model can be modified to incorporate intracellular signaling cascades regulating the cell cycle and cell cycle-dependent events as was done by Jiang et. al. (46) in their multiscale model of avascular tumor growth. Cell division occurs when a proliferating cell has doubled in size and has gone through one complete cell cycle, which we take to be 18 h (60). Cell division produces two daughter cells; one daughter cell keeps the cell ID of the parent and the other is assigned its own unique ID. Because endothelial cells demonstrate an increased rate of survival in the presence of VEGF (61), endothelial cell death is not considered in the model.

Our model also distinguishes between tip and stalk cell phenotypes (19). A tip cell is defined as the leading endothelial cell and when activated by VEGF, the tip cell migrates chemotactically using the matrix fibers for support. The tip cell is also capable of degrading the matrix fibers, thereby establishing local adhesion gradients and further promoting its migration through the stroma (23,24). Proliferation occurs behind the tip cell (17,27) and this phenomenon is captured by allowing those stalk cells to proliferate. We further assume that if the cell is proliferating, it cannot move chemotactically (17,19,35) and vice versa. The remaining stalk cells, as long as they are VEGF-activated, only move in response to cell-cell and cell-matrix adhesion, and through random membrane fluctuation.

Hybridization: interfacing the discrete and continuous models

The continuous model describing the VEGF profile and the discrete model of cellular dynamics are used as initial conditions for each other at every time step to produce a coupled system of extra- and intercellular dynamics. At time zero, the steady-state solution to Eq. 1 defines the initial VEGF profile used in the discrete cellular model. Within the discrete model, each endothelial cell uniquely responds to the amount of VEGF present by deciding whether there is sufficient VEGF to become activated. VEGF must be present in quantities above a threshold level, v_a, for endothelial cell activation to occur. Once activated, each individual endothelial cell decides whether it is a tip cell and will migrate and degrade the ECM, or if it is a proliferating cell, and will grow and divide. After the discrete model evolves through one Monte Carlo step in time, the function for endothelial cell VEGF uptake and binding, $B(x, y, V)$, is rederived based on the new distribution of endothelial cells on the lattice. A new spatial profile for VEGF at the next time step is obtained by solving Eq. 1 using the updated function $B(x, y, V)$. The lattice is then updated with the new VEGF profile. As the continuum and discrete models feed-back on each other, each endothelial cell responds to its evolving microenvironment.

Parameters

Whenever possible, we take parameters from experimental data. A list of all parameter values used in our model is provided in Table 1, including references. If no reference is given, the parameter is a relative value chosen to emulate observed phenomenological behaviors. By equating the time it takes an endothelial cell to divide during the simulation with the endothelial cell cycle duration of 18 h, we calibrate Monte Carlo steps to real time units. In the simulations, one Monte Carlo step is equivalent to 1 h.

The value for endothelial cell activation v_a is based on our numerical solutions to Eq. 1 and is chosen to activate the initial endothelial cell. A smaller relative value for $J_{\tau,\tau'}$ establishes a stronger cell surface bond. Endothelial cells will bind more tightly to each other than they will with other constituent types, whereas interstitial fluid has very little binding affinity. The membrane elasticities, γ_τ, are chosen to reflect the relative compressibility of the constituent. A larger value makes it more difficult for a constituent to deviate from its target volume and consequently more difficult to invade. Interstitial fluid is relatively easy to invade compared to the tissue-specific cells. The chemotactic potential, μ_σ, is chosen so that its contribution to total energy is on average equal to the contribution to total energy due to cell growth.

RESULTS

Realistic capillary sprout morphology captured

Fig. 3 depicts a typical simulation demonstrating the model's ability to reproduce realistic capillary sprout morphologies. So that we could attribute any changes in sprout morphology directly to the mechanism or parameter being tested, unless otherwise noted, all simulations used the same parameter set, initial configuration of matrix fibers and tissue cell distribution, and follow the assumptions described in the modeling section. Sprout migration is facilitated as the tip cell degrades the matrix fibers and effectively migrates via haptotaxis up these local adhesion gradients. Comparing simulations with and without ECM degradation, we found that tip cell ECM degradation increased the average rate of sprout extension toward the tumor by 5%, a small but statistically significant effect. The resulting morphology of the capillary sprout is determined by several mechanisms: tip cell migration toward positive VEGF and adhesion gradients, cellular adhesion to the ECM, and competition for space. Coordination of or

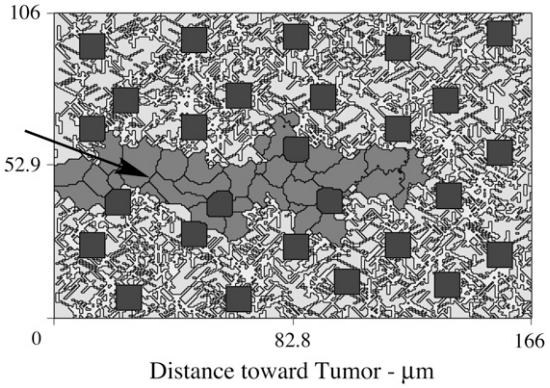

FIGURE 3 Representative simulation showing the model's ability to reproduce realistic capillary sprout morphologies. Sprouts migrate along matrix fibers up chemical gradients of VEGF. The structure of the matrix guides sprout migration and affects cell shape and orientation. The arrow identifies a cell that has elongated due to chemotactic forces and adhesion to the matrix. Parameters used are given in the parameter table except $\gamma_e = 0.7$ and $\gamma_t = 0.8$. Snapshot at 16.6 days.

competition among these mechanisms affects cell shape and orientation and can be readily observed during movies of the simulations (Supplementary Material, Movie S1). For instance, interplay between haptotaxis and chemotaxis can result in endothelial cell elongation, a characteristic cell shape for migrating cells, without needing a rule prescribing an elongated cell shape as was done in Merks et al. (59) (*arrow* in Fig. 3).

Whenever possible, we make every effort to compare cell and sprout dynamics and morphologies observed during simulations with observations from experimental assays. On average the capillary sprouts are 14.2 ± 2.44 μm (mean $\pm$ SD) in diameter and 1–2 cells wide, which compares quantitatively well to VEGF-induced vessel diameters reported in the literature (32,64). We have quantified and report the rates of sprout extension under various simulation conditions. Sprout length is determined by measuring the distance from the center of mass of the initial endothelial cell at the base of the sprout to the tip cell's center of mass at the end of the simulation. Average sprout extension velocity is then calculated as the final sprout length over time. Sprout extension rates are presented and discussed in a subsection below.

In the Introduction, several key hypotheses were formulated that were driven by confusing or conflicting results from empirical data. In the following subsections, we use our model to test these hypotheses by relaxing the relevant baseline assumption(s) set forth in the model description.

Local VEGF gradient influences capillary morphology

Recent studies have focused on the role of various VEGF isoforms in cellular function (19,49) and morphogenesis (32) and have found that VEGF in soluble versus bound form has a different effect on vascular appearance. There is evidence that steep VEGF gradients can be generated due to either high matrix binding affinity isoforms or as a result of additional soluble VEGF cleaved from the matrix (19,32,65). Since we model capillary sprout formation starting from a single cell, cell densities in our simulations are very low. Our numerical solutions to Eq. 1 show that cell uptake of diffusible VEGF for low cell densities has only a very slight effect on the chemical profile at any time. Consequently, only very shallow gradients of freely diffusible VEGF are established. Other mathematical models of angiogenesis (37,45) have simulated steep chemical gradients, but these are formed strictly as a result of VEGF consumption by a large number of endothelial cells. In addition, different tumor geometries (linear versus circular) have been simulated which also produced different VEGF gradients (43). However, all of these models focus on the effects of VEGF gradients on capillary network development and vascular patterning. They were not able to explore the effects of different VEGF gradients on individual cells (sprout stalk and tip cells) or on changes in sprout morphology that occur as a result of single cell dynamics. Using our model, we investigate the effects of different VEGF gradient profiles on cellular function and how cellular function affects sprout morphology.

In this investigation, we do not explicitly model different isoforms or the binding of VEGF to the matrix. Instead, shallow VEGF gradients are constructed by assuming endothelial cells bind a diffusible VEGF isoform. The resulting gradients are very shallow (Fig. 4 *a*). To mimic a VEGF isoform that is sequestered in the ECM, we begin with the same initial VEGF profile but do not provide a source of VEGF as before. Consequently, once an endothelial cell binds to and internalizes a VEGF molecule, VEGF is depleted over time, thereby establishing steep local concentration gradients (Fig. 4 *c*). As in our baseline simulations, each cell decides independently whether or not it has enough VEGF to become activated, v_a. Now an activated cell additionally decides whether there is enough VEGF present to stimulate proliferation, v_p. We no longer specify a proliferating region just behind the sprout tip, but allow instead VEGF concentration dependent endothelial cell proliferation (19). No experimental data is available for the threshold amount of VEGF required for proliferation, therefore we choose a value to stimulate proliferation ~48 h after the initial cell began migrating into the stroma (17,27). If there is insufficient VEGF, a cell will deactivate and become inert.

Fig. 4 *b* shows the endothelial cell response to soluble VEGF. As the sprout grows, a greater number of endothelial cells are activated and stimulated to proliferate (Supplementary Material, Movie S2). Because more cells are growing, the entire sprout is on average 46% larger and the sprout is more invasive. The average diameter of the sprout was 60 μm. Furthermore, because only shallow gradients are formed, the tip cell does not have strong directional preference from chemoattractant gradients. The resulting morphology is

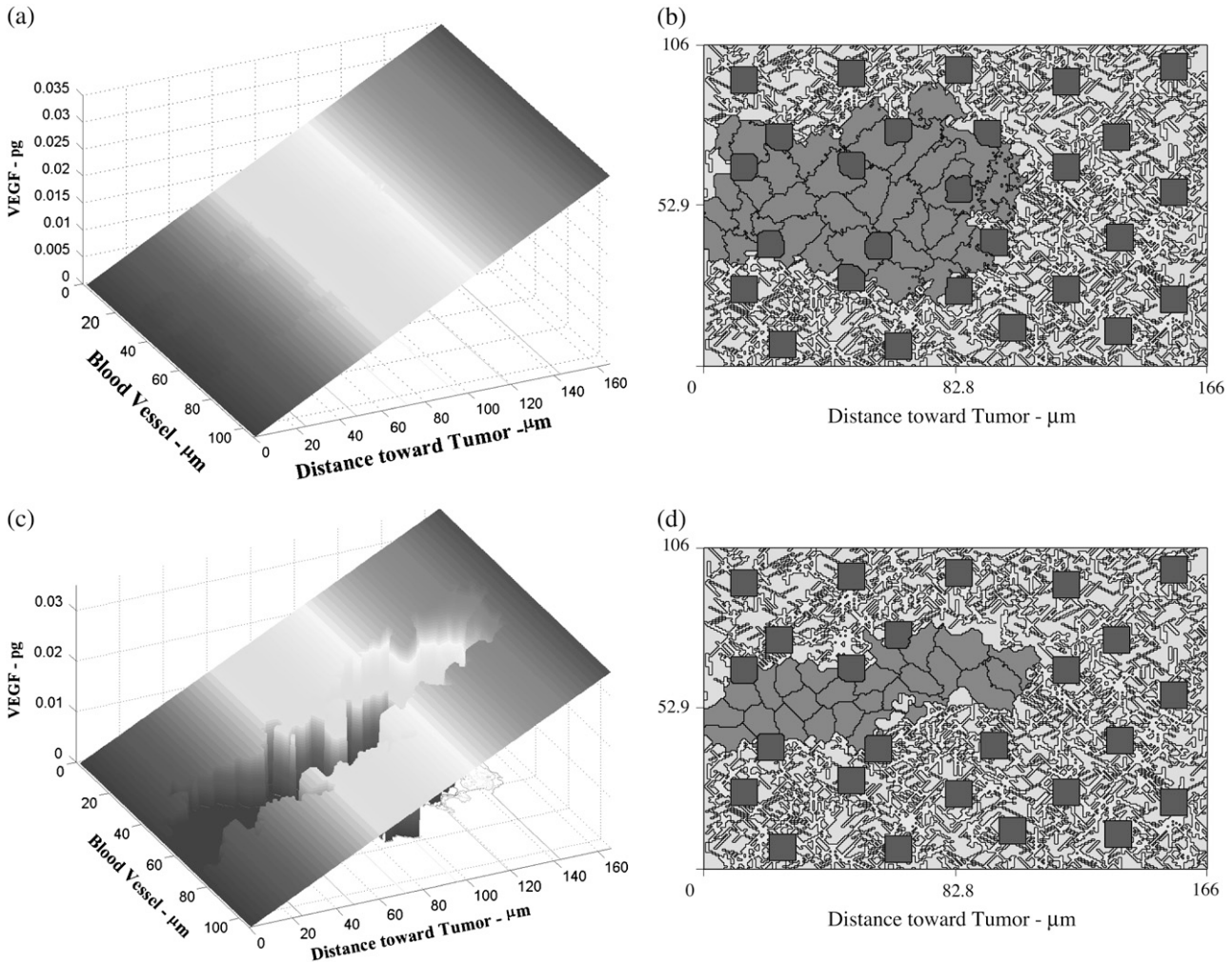

FIGURE 4 The markedly different capillary sprout morphologies that result from shallow (*a*) versus steep (*c*) VEGF gradients. Swollen, invasive sprouts result from shallow VEGF gradients that develop when freely soluble VEGF is expressed (*b*), whereas when matrix-bound VEGF isoforms are assumed, steep gradients develop and result in narrower capillary sprouts (*d*). Both results concur with the experimental observations of Lee et al. (32). Parameters are given in the parameter table. Snapshots at (*b*) 9.4 and (*d*) 16.6 days.

a swollen sprout, a morphology consistent with vascular hyperplasia (32). We also see lateral and backward cell movement following adhesive gradients. Backward migration, or migration back toward the parent vessel, is an observed phenomenon in vivo (see Fig. 1 in (45)) and was also numerically simulated in Sun et al. (45). Fig. 4 *d* depicts the capillary morphology that results from steep extracellular gradients of matrix-bound VEGF. The morphology is strikingly different. As VEGF is depleted, there is a reduction in the size of the proliferating region and some cells eventually became inactive. Additionally, steep gradients provide strong migrational cues to the tip cell and the result is a less invasive sprout with an average diameter of 20 μm. For shallow gradients, increasing the proliferating threshold effectively introduced a delay in the dynamics; however, in both cases, the ultimate capillary morphology is unchanged.

The morphologies we observe agree well with the experimental observations in Lee et al. (32), which tested the angiogenic responses to different VEGF isoforms in vivo. They demonstrated that endothelial cell receptor activation by soluble VEGF induced significant cell proliferation and broad invasion of the stroma (vessel diameter of 109 μm), whereas receptor activation by matrix-bound isoforms resulted in filopodia extension, limited stromal invasion, and cell-cell associations consistent with sprouting angiogenesis (vessel diameter of 15 μm). Moreover, endothelial cells in shallow VEGF gradients lose their directional guidance cues (19). This observation agrees with the results of Gerhardt et al. (19), where tip cell filopodia lost their polarity and excessive filopodia extend from stalk cells in response to shallow gradients of VEGF in transgenic mice expressing only $VEGF_{120}$.

Average rates of sprout extension are affected by proliferating region and cooperation of cellular functions

As discussed previously, experimental models have reported conflicting results regarding the precise region of proliferating cells during angiogenesis. We use our model to investigate the effects of various proliferating regions on capillary morphology and on the average rate of sprout extension toward the tumor. We look at capillaries that develop with proliferation occurring:

1. Only at the tip of the growing sprout.
2. Immediately behind the sprout tip.
3. Three cell lengths behind the advancing tip.
4. At the base of the sprout.

Because newly formed sprouts have not yet resynthesized a basement membrane, proliferation in these different regions is biologically feasible. Empirical evidence quantifying the distribution of cell divisions during sprout formation showed that proliferation can occur at the tip, behind the tip, and at the base of newly formed sprouts (33). As in our baseline simulations, if a cell is proliferating, it does not move chemotactically. We run all simulations for the same duration and use the same parameter set.

Among the proliferating regions tested, we find no marked differences in sprout morphology. Fig. 5 shows the resulting sprouts when proliferation occurred at the base (*top inset*) and at the tip (*lower inset*) of the sprout. Fig. 5 also shows the relationship between the proximity of the proliferating region to the tip and sprout extension speeds toward the tumor. The data indicate that as the proliferating region moves further away from the migrating tip, the average rate of sprout extension toward the tumor increases. These results suggest some interplay or competition between the mechanical or biochemical forces exerted by the migrating tip and the proliferating cells. Migrating cells move toward the source of chemoattractant and the cells adhered to it are pulled along. On the other hand, proliferating cells do not necessarily grow directly toward the chemical source. This is because it requires less energy for the cells that make up the capillary sprout to grow into matrix and fluid than to invade the space occupied by other cells. In addition, a proliferating cell does not migrate and consequently anchors neighboring cells via cell-cell adhesion. When a proliferating cell is adjacent to a migrating cell, each phenotype has to overcome the forces exerted by the other. However, once the proliferating region is far enough away, there is no statistically significant change in sprout extension speed, suggesting that the forces exerted by each phenotype have only short-range effects.

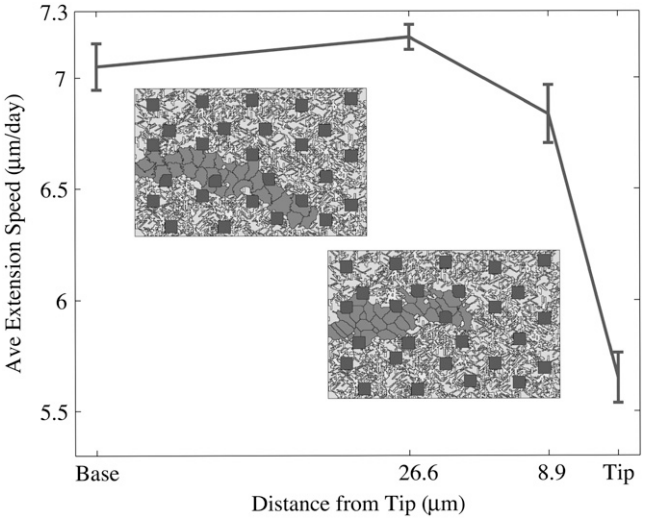

FIGURE 5 The relationship between the average rate of sprout extension and the location of the proliferating region. The further the proliferating region from the migrating tip, the faster the average rate of sprout extension due to the interplay between the chemotactic forces exerted by the migrating tip and competition for space by the proliferating cells. Error bars represent standard deviations from the mean using a sample of 12 simulations. Parameters used are as given in the parameter table except $\gamma_e = 0.7$ and $\gamma_t = 0.8$.

To investigate the validity of this explanation, we perform a numerical experiment identical to Experiment 1, above, except that migration and proliferation are no longer independent and exclusive cellular events. It has been shown empirically that proliferation and migration are not isolated cellular functions (33). We find that when proliferating cells also move chemotactically, the average rate of sprout extension increases to 7.7 μm/day, significantly faster than any of the speeds observed for all proliferating regions tested. This rate represents a 36.5% increase above the rate observed in Experiment 1 and a 7.4% increase over the fastest average speed observed (Experiments 1–4). This finding supports the view that proliferating and migrating cells exert short-range competing forces on each other and further suggests that coordination of these cellular functions could have a significant effect on the rate of capillary extension. Our examination does not rule out the possibility that multiple proliferating regions may exist.

Stroma composition and ECM structure: mechanisms for capillary sprout branching and anastomosis

As shown in Fig. 6 *a*, our model is able to reproduce branching structures. An exciting feature of this model is that branching occurs naturally as a result of known cellular and molecular level dynamics, not as a result of predefined probabilistic rules. To our knowledge, no other model has simulated sprout branching without a priori prescribing a phenomenological rule. Movies of capillary sprout evolution are evaluated to examine the possibility that heterogeneities in the stroma induced branching (Supplementary Material, Movie S3). We observe that the direction of sprout migration is predominantly determined by chemotaxis and endothelial cell adhesion to and movement along the matrix fibers. As

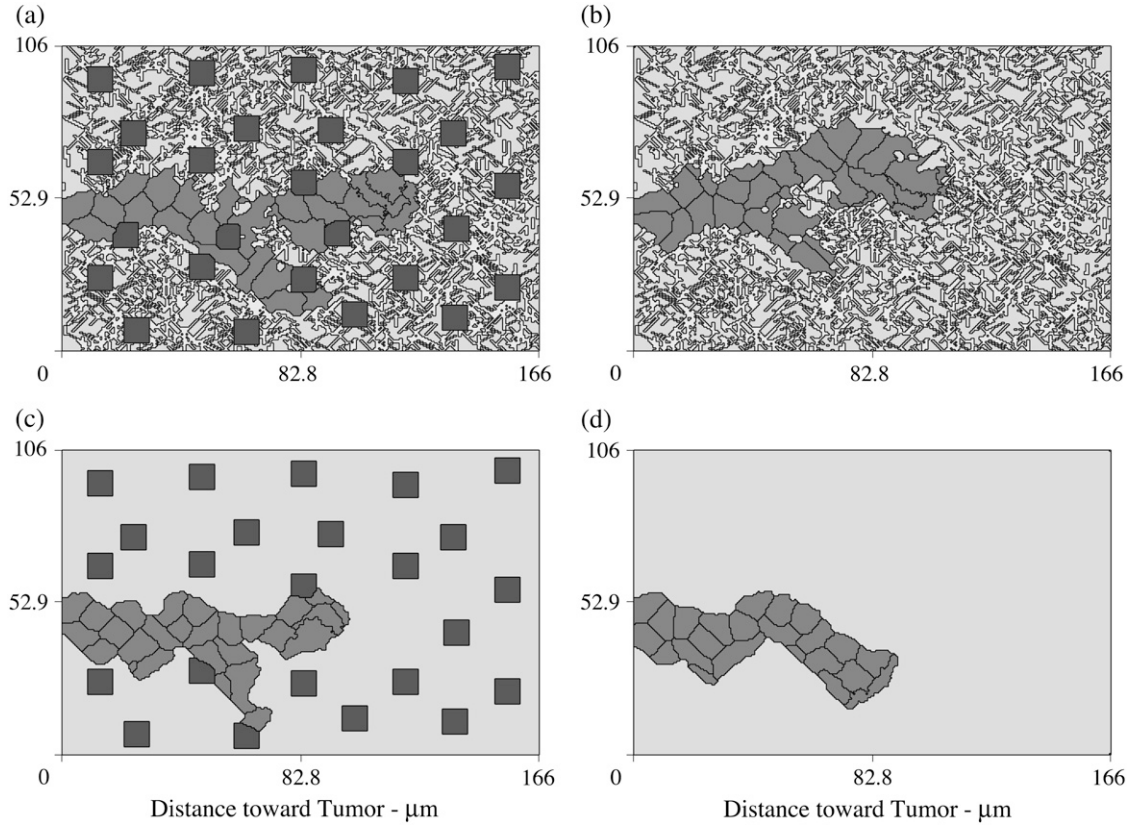

FIGURE 6 Numerical simulations ruling out the possibility that branching is induced solely by the tessellated structure of the stroma. For an identical parameter set, (*a*) depicts a branch emerging from the main capillary as a result of anisotropies in the stroma, (*b*) demonstrates that the structure of the matrix fibers alone can induce branching, and (*c*) shows branch formation induced by resident tissue cells. No branching occurs in a homogeneous extracellular environment due to a loss of adhesive guidance cues (*d*). Parameters are given in Table 1. Results suggest two plausible mechanisms for sprout branching: the resistance created by other cells in the tissue and the structure of matrix fibers. Snapshot at 16.6 days.

the leading cells encounter variable matrix densities and other stromal cells, the sprout changes direction to find a path of lower resistance through the stroma. Regions of higher density matrix impose a barrier to forward migration, whereas regions of relatively low densities do not provide enough adhesion or cellular support for migration. Both extremes cause the sprout to change direction and lead to more tortuous sprout morphologies. We hypothesize that anisotropies in matrix fiber structure or intercellular pressure by tissue cells provides an opportunity for the redirection of the entire sprout or of individual cells. It is possible that it is this redirection or migration of individual cells that leads to branch formation. Whether or not a branch emerges depends on the combination of local forces acting on the individual cells. Forces induced by cell-matrix adhesion coupled with chemotaxis or intercellular pressures may facilitate cellular migration away from the main body of the developing sprout. Compared to other models of tumor-induced angiogenesis that simulate the ''brush border'' effect (43,45), which is an increased incidence of branching as the sprout approaches the tumor (48), the length of our computational domain is much shorter. Consequently, we do not expect to reproduce the brush border effect captured on longer length scales (1–2 mm) that allow multiple branching points to form.

To investigate the possibility that the tessellated structure of the stroma may have generated the observed capillary sprout branching, we conduct three additional numerical experiments: sprout formation 1), in the absence of tissue-specific cells; 2), in the absence of matrix fibers; and 3), within a homogeneous extravascular environment (no matrix and no tissue cells). We then examine the effects of altering the compressibility of the tissue cells. All simulations are identical except for the absence of tissue cells or matrix fibers. Fig. 6, *b–d*, shows representative final images from numerical experiments 1–3, respectively. In the first experiment, we completely remove the tissue cells from the stroma. Fig. 6 *b* shows that a branch still emerges, but in this case it develops solely in response to chemotactic gradients and cell-matrix adhesion. We then observe sprout formation in the absence of matrix fibers (Fig. 6 *c*). In this simulation, the tip cell is slowed by and deforms itself to accommodate a tissue cell. The resistance from the tissue cell is enough to redirect the leading cells and the sprout splits forming a

branch (Supplementary Material, Movie S3). In the last experiment, we simulate sprout formation in the absence of both tissue-specific cells and matrix fibers (Fig. 6 *d*). This experiment examines sprout migration due to chemotaxis and cell-cell adhesion alone. As may be expected, the sprout is more linear and cells appear more elongated due to the effects of chemotaxis, but the sprout is also larger in diameter and much slower (see Table 2). This is because the absence of an extracellular matrix results in a loss of adhesive guidance cues generally provided by the matrix fibers and consequently a decrease in tip cell polarity. Interestingly, we also observe greater persistence in sprout migration, that is, once the sprout is oriented, it does not easily change its direction. This is not surprising when presented with the extensive evidence that the ECM plays a crucial role in sprout guidance and morphology. In support of our hypothesis that inhomogeneities in the stroma are a mechanism for branching, we do not see sprout branches in the absence of variable stromal structure. Table 2 compares the average extension speeds and average sprout diameters for the various stromal compositions. The rates of sprout extension for sprouts developing without an extracellular matrix are significantly slower than those that develop with the additional migratory cues provided by the matrix fibers. Average extension speeds and average diameters are not statistically different for sprouts growing in the absence of an ECM. The average rate of sprout extension due to chemotaxis is 5.33 μm/day. The possibility for endothelial cells to additionally employ extracellular matrix fibers for migration results in an 18–28% increase in average extension speed. In another series of numerical experiments, varying the compressibility of the tissue cells does not result in any significant differences in capillary development (results not shown).

Fig. 7 shows the development of capillary sprouts from five endothelial cell buds (Supplementary Material, Movie S4). As the sprouts extend toward the tumor, two neighboring sprouts anastomose forming a loop. It should be noted that anastomosis is also the result in the literature (43,45), where the lateral motion of the sprout tip is influenced by positive adhesive gradients created by endothelial cell fibronectin uptake in the literature (43,45) and additionally by matrix heterogeneities in Sun et al. (45). In our model, the lateral motion of the sprouts similarly occurs as a result of local adhesive gradients that naturally exist due to matrix anisotropies, but also occurs as a result of the positive gradients created through endothelial cell matrix degradation. Sprout migration is further directed by endothelial cell surface binding to matrix fibers and by the resistance from extravascular tissue cells. When two neighboring sprouts encounter each other, they may or may not merge to form a loop. That is, whether or not anastomosis will occur depends on the dynamics of individual cell-cell and cell-matrix binding, coupled with chemotactic and haptotactic gradients. As with branching, loop formation emerges naturally as a collective result of single cell behaviors and is a preferred lower energy state structure. We would like to point out that as the sprouts that form loops mature, blood would begin to circulate and the forces associated with the flow of blood could cause side branching. Consistent with Kearney et al.

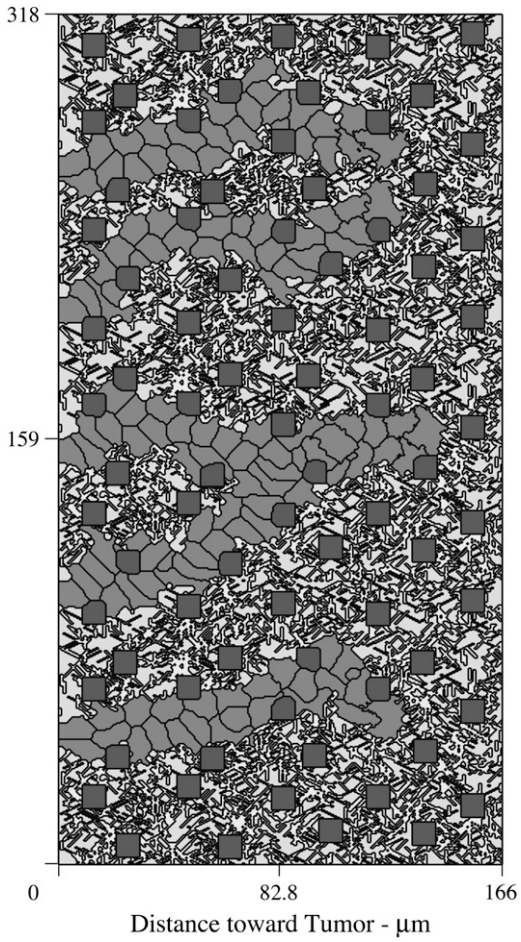

FIGURE 7 The development of capillary sprouts from five endothelial cell buds. Two neighboring sprouts have fused together forming a loop, a process known as anastomosis. In this simulation, anastomosis was a preferred lower energy state structure given the known physical dynamics at the cellular level (Supplementary Material, Movie S4). Parameters are given in the parameter table. Snapshot at 16.6 days.

TABLE 2 Table comparing average migration speeds and average sprout diameters for different stromal compositions

Stromal composition	Avg. migration speed mean ± SD error (μm/day)	Avg. sprout diameter mean ± SD error (μm)
No fibers, no tissue cells	5.33 ± 0.075	19.29 ± 0.26
Tissue cells only	5.41 ± 0.074	19.08 ± 0.46
Matrix fibers only	6.33 ± 0.131	14.41 ± 0.26
With fibers and tissue cells	6.84 ± 0.131	14.20 ± 0.70

Averages are computed from a sample of 12 simulations with identical parameters and initial conditions. Average migration speed of the sprout is calculated as sprout tip displacement at the end of the simulation from the initial endothelial cell per time.

(33), our simulations show that blood flow is not necessary for tip branching and anastomosis.

These studies indicate that the anisotropic structure of the matrix fibers strongly influences the direction and morphology of the migrating capillary sprout. We additionally find that resistance from tissue cells and endothelial cell adhesion to matrix fibers during endothelial cell migration, both alone and in concert, is sufficient to cause branching and anastomosis to occur. We also show that regions of either high density or very low-density matrix alone can inhibit and redirect endothelial cell movement inducing capillary sprout branching. These results suggest that the anisotropy of the matrix fibers and the composition of the stroma may be important mechanisms leading to capillary sprout branching and anastomosis.

SENSITIVITY ANALYSIS

The sensitivity of the results to the particular parameter set chosen is studied by varying one parameter at a time. First, holding matrix fiber density constant, we randomly generate alternative ECM structures as described in Modeling the Stroma and Extracellular Matrix, and find that our results do not qualitatively change. Further studies show that the results are insensitive to changes in γ_f, γ_m, and γ_t but cell size depends on γ_e and cell shape depends on J_{em}. Larger values of γ_e (requires more energy to grow) yield smaller cells, and the smaller the value for J_{em} (stronger bond), the more elongated the cell. Varying the chemical potential, μ_σ, affects both shape and size. As μ_σ is increased by an order of magnitude, the cells become much larger and more elongated and sprout extension is rapid and pervasive. Increasing μ_σ increases the ratio of chemotactic potential to growth and adhesion and causes the system energy changes to be dominated by the effects of chemotaxis. Very little difference is seen in cell size and shape until μ_σ is decreased three orders of magnitude, at which point cells become rounder and sprout extension is stunted. Significantly decreasing μ_σ is equivalent to having no chemotactic forces in the system. The results are not sensitive to the value of kT until this value is increased more than two orders of magnitude. At this point the cells break up because larger values of kT correspond to greater cell membrane fluctuations.

DISCUSSION

Tumor angiogenesis is an important step in cancer development. Recent experimental advances highlight the increasingly complex and still largely unresolved mechanisms driving tumor angiogenesis. We formulate specific hypotheses relevant to the investigation of biomechanical and biochemical mechanisms. We present a cell-based model of tumor angiogenesis incorporating endothelial cells, stroma tissue, ECM, and interstitial fluid, as well as VEGF dynamics. This model reflects a realistic representation of the complex and dynamic nature of the tumor microenvironment with multiple cell types and reciprocal cellular and molecular interactions. We demonstrate its capacity to capture realistic dynamics and capillary sprout morphologies, such as preferential sprout migration along matrix fibers, cell elongation, and more complex events, such as branching and anastomosis, that occur during angiogenesis. Our model provides a framework for incorporating biochemistry and physics in investigations of mechanism.

We provide evidence that differences in the matrix-binding affinity of VEGF isoforms could affect the VEGF profile and show that vastly different capillary morphologies result in the presence of steep versus shallow extracellular chemical gradients. Our model reproduces narrow sprouts in the presence of steep VEGF gradients and swollen sprout formation due to well-distributed concentrations of VEGF; both morphologies and mechanisms are consistent with those observed empirically by Lee et al. (32) and Gerhardt et al. (19). These results emphasize the importance of capturing not only the correct chemical profile, but also the correct mechanisms inducing the extracellular chemical profiles. Models of angiogenesis inducing steep gradients as a result of VEGF uptake by a large number of cells may be neglecting a vital mechanism responsible for the modulation of endothelial cell function and vascular form. To date, mathematical models have focused on the effects of tumor-secreted VEGF in a freely diffusible form. If we hope to understand the mechanisms regulating capillary formation, models must incorporate other VEGF isoforms and allow for VEGF binding to and liberation from the ECM. Using this model as a starting point, we can examine the role of different VEGF isoforms on the spatial profile of bio-available VEGF and in regulating cellular functions and test the hypothesis that the proteolytic release of matrix-bound VEGF isoforms naturally defines a proliferating region of endothelial cells and causes local growth differentials.

The underlying mechanisms by which a proliferating region is established during angiogenesis are still at large. We identify biological models of angiogenesis that report cell proliferation from distinctly different regions of a developing sprout. Using our model, we explore the effects of various proliferating regions on capillary sprout growth. Results from our numerical simulations show that as the proliferating region moves further from the sprout tip, sprout extension is more rapid due to diminishing competing intercellular forces. Results also show that the location of the proliferating region does not influence sprout morphology. We demonstrate that capillary sprout extension is significantly more rapid when cellular functions (migration and proliferation) are not mutually exclusive. Our results highlight just how tightly regulated the processes involved in angiogenesis are and indicate the need for studies of the relative importance of chemotaxis and proliferation on capillary development. Furthermore, in these numerical experiments, the proliferating region is a fixed distance from the tip throughout the simulation; however, in vivo it may be that as the sprout extends

toward the tumor, it is the proliferating region that remains fixed—that is, the region lags further and further behind the advancing tip (34). Coupled with our finding that sprout extension speed is affected by the location of the proliferating region, this could possibly explain the increase in capillary migration speeds seen empirically as capillary networks approach the tumor.

The composition and structure of the stroma through which the new capillaries must grow to reach the tumor are highly tissue-dependent. We examine the role of tissue inhomogeneities by explicitly modeling the interactions between endothelial cells and the stroma, specifically the matrix fibers, resident tissue cells, and interstitial fluid. Our studies reveal that local anisotropies in the stroma, such as variable matrix fiber density and the presence of other tissue cells, influence sprout migration and morphology during angiogenesis and may be mechanisms for sprout branching and anastomosis. Although the morphology of branching and anastomosis has been fully described (17,33), little is understood of the cellular and molecular mechanisms inducing the formation of these sprout structures. In our model, anastomosis and branching occur because they are preferred lower energy state structures given the chemical and mechanical dynamics incorporated at the cellular level. Our initial results underscore the importance of modeling cell-matrix and cell-cell dynamics and demonstrate that a cell-based physical model can help provide insight into the processes controlling angiogenesis. An in-depth study of the role of the extracellular matrix and tissue composition on sprout formation, including an investigation of the density distribution of tissue cells and matrix fibers and matrix fiber alignment, is the subject of work in progress.

At present, quantifying our results and validating our model is not a straightforward task. Measurements of microvessel densities over time, branching points/mm/time, and capillary network expansion rates exist for vascular networks that form on larger spatial scales. However, our model focuses on cell-cell and cell-matrix interactions at the very onset of angiogenesis, when the newly formed sprouts consist of only a few cells. Additionally, on the spatial scale of our model, which is significantly smaller, we do not expect multiple branch points to form. Assays and quantitative measures of early single sprout morphology under conditions that mimic the early events that occur in vivo during tumor-induced angiogenesis have not been well developed. In particular, to our knowledge there has been no systematic study of collective cell or sprout migration and morphology that quantifies the effects of chemotaxis. In addition, experimental models that measure individual cell migration rates cannot be directly compared to the rate at which a capillary sprout travels or extends toward a tumor, because cell-cell dynamics are not considered in assays of single cell motility and during sprout extension migrating cells are adhered to other cells that may be anchored to the matrix or moving in different directions.

Average speeds of in vivo and in vitro vessel growth have been reported at 0.1–0.3 mm/day (33,66). The average rate of sprout extension in our model is considerably slower. This difference can be attributed to a combination of several factors. First, in our simulations, cell proliferation occurs only in one cell. Simulating multiple proliferating regions or proliferation in multiple cells does increase the rate of sprout extension in our model. Fig. 4 *b* shows an increased sprout extension rate when there are more proliferating cells. This sprout has migrated the same distance as the sprout in Fig. 4 *d* but in only 9.4 vs. 16.6 days. However, proliferation alone does not explain the difference in sprout migration rates. Other factors that contribute to sprout extension speeds are the ECM density, cell elongation, and blood flow. Endothelial cells can elongate up to 10 times their normal length (33) and the density and alignment of matrix fibers has a major effect on cell migration rates (53). We are currently investigating the effects of cell elongation on sprout extension speeds and have measured sprout speeds through matrices of varying densities and patterns, which predict an optimal density for maximal sprout migration speeds (unpublished results). Another dynamic that has a significant impact on our sprout extension speeds is the ability to capture sheet or cohort migration of a group of cells as is observed in vascular sprouting (67). An important mechanism in both single cell and collective migration is the detachment from the ECM and subsequent retraction of the trailing edge of the cell. In our model, we have not yet incorporated the effects of ECM detachment and cell retraction. Preliminary studies of simulated single cell migration and sprout formation incorporating these cellular motility mechanisms suggest that sprout migration speeds may more than double.

SUPPLEMENTARY MATERIAL

An online supplement to this article can be found by visiting BJ Online at http://www.biophysj.org.

The authors thank M. Luisa Iruela-Arispe and Charles D. Little for valuable discussions.

This research was carried out under the auspices of the National Nuclear Security Administration of the U.S. Department of Energy at Los Alamos National Laboratory under contract No. DE-AC52-06NA25396. T.L.J. was supported in part by the Alfred P. Sloan Foundation and the James S. McDonnell Foundation. This work was performed at Los Alamos National Laboratory as part of the PhD dissertation research of A.L.B.

REFERENCES

1. Straume, O., H. B. Salvesen, and L. A. Akslen. 1999. Angiogenesis is prognostically important in vertical growth phase melanomas. *Int. J. Oncol.* 15:595–599.
2. Asahara, T., C. Kalka, and J. M. Isner. 2000. Stem cell therapy and gene transfer for regeneration. *Gene Ther.* 7:451–457.
3. Carmeliet, P., and R. K. Jain. 2000. Angiogenesis in cancer and other diseases. *Nature.* 407:249–257.

4. Leith, J. T., and S. Michelson. 1995. Secretion rates and levels of vascular endothelial growth factor in clone-a or Hct-8 human colon tumor cells as a function of oxygen concentration. *Cell Prolif.* 28: 415–430.
5. Carmeliet, P., V. Ferreira, G. Breier, S. Pollefeyt, L. Kieckens, M. Gertsenstein, M. Fahrig, A. Vandenhoeck, K. Harpal, C. Eberhardt, C. Declercq, J. Pawling, L. Moons, D. Collen, W. Risau, and A. Nagy. 1996. Abnormal blood vessel development and lethality in embryos lacking a single VEGF allele. *Nature.* 380:435–439.
6. Carmeliet, P. 2000. Mechanisms of angiogenesis and arteriogenesis. *Nat. Med.* 6:389–395.
7. Ferrara, N., and W. J. Henzel. 1989. Pituitary follicular cells secrete a novel heparin-binding growth factor specific for vascular endothelial cells. *Biochem. Biophys. Res. Commun.* 161:851–858.
8. Yancopoulos, G. D., S. Davis, N. W. Gale, J. S. Rudge, S. J. Wiegand, and J. Holash. 2000. Vascular-specific growth factors and blood vessel formation. *Nature.* 407:242–248.
9. Nör, J. E., J. Christensen, D. J. Mooney, and P. J. Polverini. 1999. Vascular endothelial growth factor (VEGF)-mediated angiogenesis is associated with enhanced endothelial cell survival and induction of Bcl-2 expression. *Am. J. Pathol.* 154:375–384.
10. Hicklin, D. J., and L. M. Ellis. 2005. Role of the vascular endothelial growth factor pathway in tumor growth and angiogenesis. *J. Clin. Oncol.* 23:1011–1027.
11. Roberts, W. G., and G. E. Palade. 1995. Increased microvascular permeability and endothelial fenestration induced by vascular endothelial growth factor. *J. Cell Sci.* 108:2369–2379.
12. Mignatti, P., and D. B. Rifkin. 1993. Biology and biochemistry of proteinases in tumor invasion. *Physiol. Rev.* 73:161–195.
13. Iruela-Arispe, M. L., P. Hasselaar, and H. Sage. 1991. Differential expression of extracellular proteins is correlated with angiogenesis in vitro. *Lab. Invest.* 64:174–186.
14. Huang, S., and D. E. Ingber. 1999. The structural and mechanical complexity of cell-growth control. *Nat. Cell Biol.* 1:E131–E138.
15. Alberts, B., D. Bray, J. Lewis, M. Raff, K. Roberts, and J. D. Watson. 2002. Molecular Biology of the Cell, 4th Ed. Garland Science, New York.
16. Senger, D. R., K. P. Claffey, J. E. Benes, C. A. Perruzzi, A. P. Sergiou, and M. Detmar. 1997. Angiogenesis promoted by vascular endothelial growth factor: Regulation through $\alpha1\beta1$ and $\alpha2\beta1$ integrins. *Proc. Natl. Acad. Sci. USA.* 94:13612–13617.
17. Paweletz, N., and M. Knierim. 1989. Tumor related angiogenesis. *Crit. Rev. Oncol. Hematol.* 9:197–242.
18. Shizukuda, Y., S. Tang, R. Yokota, and J. A. Ware. 1999. Vascular endothelial growth factor-induced endothelial cell migration and proliferation depend on a nitric oxide-mediated decrease in protein kinase $c\delta$ activity. *Circ. Res.* 85:247–256.
19. Gerhardt, H., M. Golding, M. Fruttiger, C. Ruhrberg, A. Lundkvist, A. Abramsson, M. Jeltsch, C. Mitchell, K. Alitalo, D. Shima, and C. Betsholtz. 2003. VEGF guides angiogenic sprouting utilizing endothelial tip cell filopodia. *J. Cell Biol.* 161:1163–1177.
20. Yoshida, A., B. Anand-Apte, and B. R. Zetter. 1996. Differential endothelial migration and proliferation to basic fibroblast growth factor and vascular endothelial growth factor. *Growth Factors.* 13:57–64.
21. Cao, Y., H. Chen, L. Zhou, M. Chiang, B. Anand-Apte, J. A. Weatherbee, Y. Wang, F. Fang, J. G. Flanagan, and M. L. Tsang. 1996. Heterodimers of placenta growth factor/vascular endothelial growth factor: endothelial activity, tumor cell expression, and high affinity binding to FLK-1/KDR. *J. Biol. Chem.* 271:3154–3162.
22. Waltenberger, J., L. Claesson-Welsh, A. Siegbahn, M. Shibuya, and C. H. Heldin. 1994. Different signal transduction properties of KDR and FLT1, two receptors for vascular endothelial growth factor. *J. Biol. Chem.* 269:26988–26995.
23. Stetler-Stevenson, W. G. 1999. Matrix metalloproteinases in angiogenesis: a moving target for therapeutic intervention. *J. Clin. Invest.* 103:1237–1241.
24. Hangai, M., N. Kitaya, J. Xu, C. Chan, J. Kim, Z. Werb, S. Ryan, and P. Brooks. 2002. Matrix metalloproteinase-9-dependent exposure of a cryptic migratory control site in collagen is required before retinal angiogenesis. *Am. J. Pathol.* 161:1429–1437.
25. Rafiee, P., J. Heidemann, H. Ogawa, N. A. Johnson, P. J. Fisher, M. S. Li, M. F. Otterson, C. P. Johnson, and D. G. Binion. 2004. Cyclosporin-A differentially inhibits multiple steps in VEGF induced angiogenesis in human microvascular endothelial cells through altered intracellular signaling. *Cell Commun. Signal.* 2:3.
26. Goto, F., K. Goto, K. Weindel, and J. Folkman. 1993. Synergistic effects of vascular endothelial growth factor and basic fibroblast growth factor on the proliferation and cord formation of bovine capillary endothelial cells within collagen gels. *Lab. Invest.* 69: 508–517.
27. Sholley, M. M., G. P. Ferguson, H. R. Seibel, J. L. Montour, and J. D. Wilson. 1984. Mechanisms of neovascularization. Vascular sprouting can occur without proliferation of endothelial cells. *Lab. Invest.* 51: 624–634.
28. Mantzaris, N. V., S. Webb, and H. G. Othmer. 2004. Mathematical modeling of tumor-induced angiogenesis. *J. Math. Biol.* 49:111–187.
29. Davis, G., and C. W. Camarillo. 1996. An $\alpha2\beta1$ integrin-dependent pinocytic mechanism involving intracellular vacuole formation and coalescence regulates capillary lumen and tube formation in three-dimensional collagen matrix. *Exp. Cell Res.* 224:39–51.
30. Hirschi, K. K., and P. A. D'Amore. 1997. Control of angiogenesis by the pericyte: molecular mechanisms and significance. *EXS.* 79:419–428.
31. Ferrara, N., H. Gerber, and J. LeCouter. 2003. The biology of VEGF and its receptors. *Nat. Med.* 9:669–676.
32. Lee, S., S. M. Jilani, G. V. Nikolava, D. Carpizo, and M. L. Iruela-Arispe. 2005. Processing of VEGF-A by matrix metalloproteinases regulates bioavailability and vascular patterning in tumors. *J. Cell Biol.* 169:681–691.
33. Kearney, J. B., N. C. Kappas, C. Ellerstrom, F. W. DiPaola, and V. L. Bautch. 2004. The VEGF receptor FLT–1 (VEGFR–1) is a positive modulator of vascular sprout formation and branching morphogenesis. *Blood.* 103:4527–4535.
34. Hunter, W., and L. Arsenault. 1990. Vascular invasion of the epithelial growth plate: analysis of metaphyseal capillary ultrastructure and growth dynamics. *Anat. Rec.* 227:223–231.
35. Ausprunk, D. H., and J. Folkman. 1977. Migration and proliferation of endothelial cells in preformed and newly formed blood vessels during tumor angiogenesis. *Microvasc. Res.* 14:53–65.
36. Sainson, R. C., J. Aoto, M. N. Nakatsu, M. Holderfield, E. Conn, E. Koller, and C. C. Hughes. 2005. Cell-autonomous notch signaling regulates endothelial cell branching and proliferation during vascular tubulogenesis. *FASEB J.* 19:1027–1029.
37. Levine, H. A., S. Pamuk, B. D. Sleeman, and M. Nilsen-Hamilton. 2001. Mathematical modeling of capillary formation and development in tumor angiogenesis: penetration into the stroma. *Bull. Math. Biol.* 63:801–863.
38. Levine, H. A., A. L. Tucker, and M. Nilsen-Hamilton. 2002. A mathematical model for the role of cell signal transduction in the initiation and inhibition of angiogenesis. *Growth Factors.* 20: 155–175.
39. McDougall, S. R., A. R. A. Anderson, and M. A. J. Chaplain. 2006. Mathematical modeling of dynamic adaptive tumor-induced angiogenesis: clinical implications and therapeutic targeting strategies. *J. Theor. Biol.* 241:564–589.
40. Anderson, A. R. A., and M. A. J. Chaplain. 1997. A mathematical model for capillary network formation in the absence of endothelial cell proliferation. *Appl. Math. Lett.* 11:109–114.
41. Stokes, C. L., and G. A. Lauffenburger. 1991. Analysis of the roles of microvessel endothelial cell random motility and chemotaxis in angiogenesis. *J. Theor. Biol.* 152:377–403.
42. Lowe, P. M., M. L. Lee, C. J. Jackson, S. S. To, A. J. Cooper, and L. Schrieber. 1995. The endothelium in psoriases. *Br. J. Dermatol.* 132:497–505.

43. Anderson, A. R. A., and M. A. J. Chaplain. 1998. Continuous and discrete mathematical models of tumor-induced angiogenesis. *Bull. Math. Biol.* 60:857–900.
44. Manoussaki, D. 2003. A mechanochemical model of angiogenesis and vasculogenesis. *ESAIM M2NA*. 37:581–599.
45. Sun, S., M. F. Wheeler, M. Obeyesekere, and C. W. P. Jr. 2005. A deterministic model of growth factor-induced angiogenesis. *Bull. Math. Biol.* 67:131–337.
46. Jiang, Y., J. Pjesivac-Grbovic, C. Cantrell, and J. P. Freyer. 2005. A multiscale model for avascular tumor growth. *Biophys. J.* 89:3884–3894.
47. Zawicki, D. F., R. K. Jain, G. W. Schmid-Schoenbein, and S. Chien. 1981. Dynamics of neovascularization in normal tissue. *Microvasc. Res.* 21:27–47.
48. Muthukkaruppan, V. R., L. Kubai, and R. Auerbach. 1982. Tumor-induced neovascularization in the mouse eye. *J. Natl. Cancer Inst.* 69:699–704.
49. Carmeliet, P. 2005. VEGF as a key mediator of angiogenesis in cancer. *Oncology.* 69:4–10.
50. Wang, D., R. E. Lehman, D. B. Donner, M. R. Matli, R. S. Warren, and M. L. Welton. 2002. Expression and endocytosis of VEGF and its receptors in human colonic vascular endothelial cells. *AJP–GI*. 282: 1088–1096.
51. Chaplain, M. A. J., and A. M. Stuart. 1991. A mathematical model for the diffusion of tumor angiogenesis factor into the surrounding host tissue. *IMA J. Math. Appl. Med. Biol.* 8:191–220.
52. Chaplain, M. A. J., and A. M. Stuart. 1993. A model mechanism for the chemotactic response of endothelial cells to tumor angiogenesis factor. *IMA J. Math. Appl. Med. Biol.* 10:149–168.
53. Friedl, P., and E. B. Bröcker. 2000. The biology of cell locomotion within three-dimensional extracellular matrix. *Cell. Mol. Life Sci.* 57:41–64.
54. Glazier, J. A., and F. Graner. 1993. Simulation of the differential adhesion driven arrangement of biological cells. *Phys. Rev. E.* 47:2128–2154.
55. Hogeweg, P. 2000. Evolving mechanisms of morphogenesis: on the interplay between differential adhesion and cell differentiation. *J. Theor. Biol.* 203:317–333.
56. Jiang, Y., H. Levine, and J. A. Glazier. 1998. Possible cooperation of differential adhesion and chemotaxis in mound formation of *Dictyostelium*. *Biophys. J.* 75:2615–2625.
57. Turner, S., and J. A. Sherratt. 2002. Intercellular adhesion and cancer invasion: a discrete simulation using the extended Potts model. *J. Theor. Biol.* 216:85–100.
58. Merks, R. M. H., and J. A. Glazier. 2006. Dynamic mechanisms of blood vessel growth. *Nonlinear*. 19:C1–C10.
59. Merks, R. M. H., S. V. Brodsky, M. S. Goligorksy, S. A. Newman, and J. A. Glazier. 2006. Cell elongation is key to in silico replication of in vitro vasculogenesis and subsequent remodeling. *Dev. Biol.* 289:44–54.
60. Williams, S. K. 1987. Isolation and culture of microvessel and large-vessel endothelial cells; their use in transport and clinical studies. *In* Microvascular Perfusion and Transportation Health and Disease. P. McDonagh, editor. Karger, Basel, Switzerland.
61. Gerber, H. P., K. Hillan, A. Ryan, J. Kowalski, G. Keller, L. Rangell, B. Wright, F. Radtke, M. Aguet, and N. Ferrara. 1999. VEGF is required for growth and survival neonatal mice. *Development*. 126:1149–1159.
62. Serini, G., D. Ambrosi, E. Giraudo, A. Gamba, L. Preziosi, and F. Bussolino. 2003. Modeling the early stages of vascular network assembly. *EMBO J*. 22:1771–1779.
63. Gabhann, F. M., and A. S. Popel. 2004. Model of competitive binding of vascular endothelial growth factor and placental growth factor to VEGF receptors on endothelial cells. *AJP Heart*. 286:153–164.
64. Lobov, I. B., P. C. Brooks, and R. A. Lang. 2002. Angiopoietin-2 displays VEGF-dependent modulation of capillary structure and endothelial cell survival in vivo. *Proc. Natl. Acad. Sci. USA*. 99:11205–11210.
65. Houck, K. A., D. W. Leung, A. M. Rowland, J. Winer, and N. Ferrara. 1992. Dual regulation of vascular endothelial growth factor bioavailability by genetic and proteolytic mechanisms. *J. Biol. Chem.* 267: 26031–26037.
66. Folkman, J. 1976. Vascularization of tumors. *Sci. Am.* 234:58–64.
67. Korff, T., and H. G. Augustin. 1999. Tensional forces in fibrillar extracellular matrices control directional capillary sprouting. *J. Cell Sci.* 112:3249–3258.